

# The influence of in situ pitch-angle cosine coverage on the derivation of solar energetic particle injection and interplanetary transport conditions

Neus Agueda <sup>a,\*</sup>, Rami Vainio <sup>a</sup>, David Lario <sup>b</sup>, Blai Sanahuja <sup>c,d</sup>

<sup>a</sup> Department of Physics, University of Helsinki, 00014 Helsinki, Finland

<sup>b</sup> Applied Physics Laboratory, Johns Hopkins University, Laurel, MD 20723-6099, USA

<sup>c</sup> Departament d'Astronomia i Meteorologia, Universitat de Barcelona, 08028 Barcelona, Spain

<sup>d</sup> Institut de Ciències del Cosmos, Universitat de Barcelona, 08028 Barcelona, Spain

Received 15 December 2008; received in revised form 25 May 2009; accepted 28 May 2009

## Abstract

Modelization of solar energetic particle (SEP) events aims at revealing the general scenario of SEP injection and interplanetary propagation and relies on in situ measurements of SEP distributions. In this paper, we study to what extent the LEFS60 and LEMS30 electron telescopes of the Electron Proton Alpha Monitor (EPAM) on board the *Advanced Composition Explorer* are able to scan pitch-angle distributions during near-relativistic electron events. We estimate the percentage of the pitch-angle cosine range scanned by both telescopes for a given magnetic field configuration. We obtain that the pitch-angle coverage is always higher for LEFS60 than for LEMS30. Therefore, LEFS60 provides more information of the directional distribution of the observed particles. The aim of the paper is to study the relevance of the coverage when fitting LEFS60 particle measurements in order to infer the solar injection and the interplanetary transport conditions. By studying synthetic electron events, we obtain that at least 70% of the pitch-angle cosine range needs to be scanned by the telescope. Otherwise, multiple scenarios can explain the data.

© 2009 COSPAR. Published by Elsevier Ltd. All rights reserved.

**Keywords:** Energetic particles; Monte Carlo simulations; Electron events

## 1. Introduction

In situ measurements of the pitch-angle distributions of solar energetic particles (SEPs) play an important role in the investigation of the solar particle acceleration and injection mechanisms, and the properties of their subsequent transport through interplanetary space. Modelization of SEP events aims at revealing the general scenario of SEP injection and transport and relies on in situ directional measurements of SEP distributions. Therefore, it is important to understand to what extent the observational data computed by a telescope maps the pitch-angle distri-

butions (PADs) during an SEP event. Only those events observed with high pitch-angle coverage can provide the most conclusive studies about the transport and injection history of SEPs.

Many particle experiments use the rotation of the spacecraft to measure the PADs of SEPs in interplanetary space, because it allows a single detector to scan different directions of space as the spacecraft spins. The swath of space swept out by a detector during a spin is normally divided into nearly equally spaced sectors. The number of counts recorded while scanning each sector together with the measurement of the interplanetary magnetic field (IMF) direction is used to infer the PADs of the particles or derive the anisotropies (Ng, 1985; Sanderson et al., 1985). The number of sectors determines the resolution in sampling

\* Corresponding author. Tel.: +358 9 191 50615; fax: +358 9 191 50610.  
E-mail address: [neus.agueda@helsinki.fi](mailto:neus.agueda@helsinki.fi) (N. Agueda).

the directional distribution of the incoming particle population.

In principle, a single detector is not able to provide full information of the three-dimensional SEP distribution. Hence, multiple detectors mounted at different positions with respect to the spin axis are needed, such as in the Low Energy Proton Experiment (DFH) on board *ISEE-3* (Sanderson et al., 1981) or in the three-dimensional Plasma and Energetic Particle Investigation (3DP) experiment on board *Wind* (Lin et al., 1995).

In this paper, we address the question of the role that the pitch-angle coverage of the telescope plays when trying to infer from in situ measurements the injection and transport conditions of SEPs. In Section 2 we explain how to quantify the pitch-angle cosine coverage of a telescope on board a spin-stabilized spacecraft. We focus on the study of two electron telescopes of the Electron Proton Alpha Monitor (EPAM) experiment (Gold et al., 1998) on board the *Advanced Composition Explorer (ACE)* spacecraft, i.e. the LEFS60 and LEMS30 telescopes. In Section 3, we assume an injection profile of electrons at the Sun and set the interplanetary transport conditions to simulate synthetic electron events. By taking into account the angular response of the telescope and assuming an IMF configuration we are able to transform the simulated PADs into synthetic sectorized intensities and study how spin-averaged intensity profiles change depending on the region of the PAD that the telescope is able to scan. In Section 4, we study the role of the pitch-angle coverage when deconvolving synthetic events. Section 5 summarizes the main conclusions of this work.

## 2. Pitch-angle cosine coverage

*ACE* is a spin-stabilized spacecraft orbiting the L1 libration point. The spin axis of the spacecraft points within  $20^\circ$  of the Sun and the spin period is of 12 s (Gold et al., 1998). As the spacecraft spins, the detectors sweep out swaths of space, providing information of the SEP directional distribution. The space scanned by each detector during one rotation is divided into nearly equally spaced sectors.

Of particular interest to this study are the LEFS60 and LEMS30 electron telescopes of the EPAM experiment. The LEFS60 telescope measures near-relativistic (45–312 keV) electrons in four energy channels. The detector has a full-cone opening angle of  $53^\circ$  and points at  $60^\circ$  from the spacecraft spin axis. As the spacecraft spins, the measurements are divided into eight sectors, each  $45^\circ$  wide (Gold et al., 1998). Similarly, the LEMS30 telescope measures near-relativistic (38–315 keV) electrons in four energy channels. The detector has a full-cone opening angle of  $51^\circ$  and points at  $30^\circ$  from the spacecraft spin axis. This telescope provides measurements into four sectors, each  $90^\circ$  wide (Gold et al., 1998).

The directions scanned by each sector and their relative probability can be estimated by calculating the angular response of a sector. Agueda et al. (2008) presented a

method to calculate the angular response of the sectors scanned by a detector on board a spin-stabilized spacecraft, such as the sectors scanned by the LEFS60 and LEMS30 detectors. Fig. 1 sketches the solid angle encompassed by the LEFS60 telescope projected onto a sphere and the approximate definition of the sectors. In the spacecraft coordinate system,  $z$  is the spacecraft spin axis and the  $x$ – $y$ -plane is perpendicular to the spin axis. Note that the directions scanned by a given sector remain constant in the spacecraft coordinate system. The pitch-angle cosine of a particle,  $\mu$ , is defined as the cosine of the angle  $\alpha$  between the particle velocity and the magnetic field vector;  $\mu = \cos \alpha$ . Then, the pitch-angle cosine of the particles scanned by a sector depend exclusively on the magnetic field vector direction. We define a generic IMF vector in the spacecraft coordinate system given by the unit vector  $\vec{B} = (1, \theta_B, \phi_B)$  expressed in spherical coordinates where  $\theta_B$  is the polar angle and  $\phi_B$  is the clock-angle. As can be seen from Fig. 1, a change in  $\theta_B$  produces a change in the range of  $\mu$  swept by the telescope. Whereas a change in  $\phi_B$ , modifies the range of  $\mu$  scanned by each sector but it does not change the total  $\mu$ -range scanned by the telescope.

Using the same grid of directions  $(\theta, \phi)$  as in Agueda et al. (2008) for the calculation of the angular response function of a sector, we can calculate a matrix of pitch-angle cosines,  $\mu_{jk} = \mu(\theta_j, \phi_k, \vec{B})$ , for a given orientation of the IMF vector. Here  $\mu_{jk}$  is a  $180 \times 360$  matrix since  $(\theta_j, \phi_k) \in [j\alpha, (j+1)\alpha] \times [k\alpha, (k+1)\alpha]$ , with  $\alpha = 1^\circ$  and  $j \in [0, 179]$ ,  $k \in [0, 359]$ . If  $R_{jk}^s$  is the angular response matrix of sector  $s$ , we can derive the view boundaries of the sector, that is, the highest and the lowest  $\mu$  values scanned, by extracting the maximum and the minimum  $\mu$  values of the  $\mu_{jk}$  matrix that have a non-zero response. The highest and lowest  $\mu$  values from all the sectors are then the maximum and the minimum  $\mu$  values scanned by the telescope.

Using this procedure, we can calculate the view boundaries of the sectors as a function of the magnetic field vector orientation. The right diagram in Fig. 1 shows the view boundaries of the two limiting sectors of the LEFS60 telescope when  $\phi_B = 60^\circ$ . As a function of  $\theta_B$ , it shows the highest and lowest  $\mu$  values scanned by two different sectors which are represented by solid and dotted curves, respectively. When  $\theta_B = 0^\circ$  or  $\theta_B = 180^\circ$  all sectors scan the same range in  $\mu$  due to the symmetry of the system.

We define the pitch-angle cosine coverage of the telescope,  $\mu$ -co, as the percentage of the pitch-angle cosine range scanned by the telescope for a given magnetic field configuration. Thus,

$$\mu\text{-co} = \frac{1}{2}(\mu_{\max} - \mu_{\min}) \times 100\% \quad (1)$$

Note again that the pitch-angle cosine range covered by the telescope only depends on  $\theta_B$  because the system is symmetric with respect to  $\phi$ . Fig. 2 shows the pitch-angle cosine range covered by the LEFS60 (solid) and the LEMS30 (dashed) telescopes and the  $\mu$ -co of the telescopes as a func-

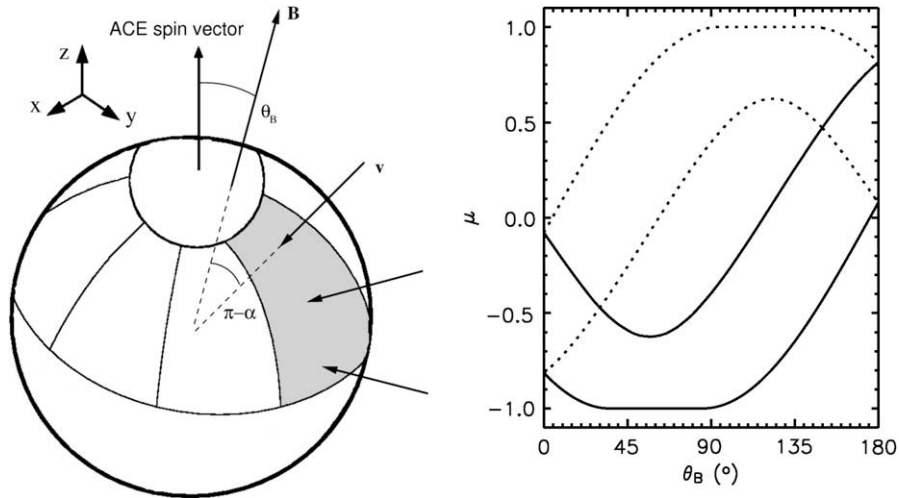


Fig. 1. Left: Solid angle encompassed by the LEFS60 telescope projected onto a sphere. Generic magnetic field vector,  $\vec{B}$ , in the spacecraft coordinate system;  $\theta_B$  denotes the polar angle. Particles measured by one of the sectors with pitch-angle cosine  $\mu = \cos \alpha$ . Right: Highest and lowest  $\mu$  scanned by the two limiting sectors (solid/dotted curves) of the LEFS60 telescope as a function of the polar angle,  $\theta_B$ , of the IMF vector when  $\phi_B = 60^\circ$ .

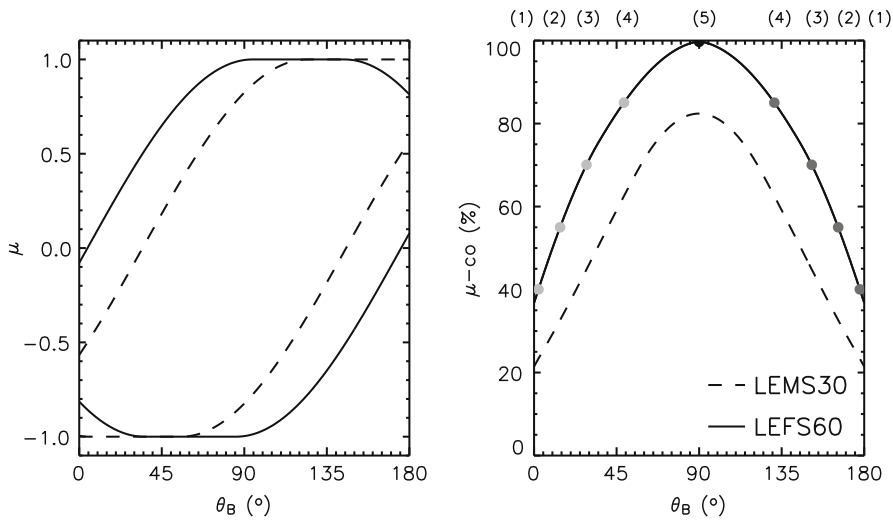


Fig. 2. Left: Highest and lowest  $\mu$  scanned by the LEFS60 (solid curves) and the LEMS30 telescope (dashed curves) as a function of the polar angle,  $\theta_B$ , of the magnetic field vector. Right: Pitch-angle cosine coverage ( $\mu$ -co) of the LEFS60 and LEMS30 telescopes as a function of  $\theta_B$ . The dots indicate several magnetic field configurations, with LEFS60  $\mu$ -co equals to 40% (1), 55% (2), 70% (3), 85% (4) and 100% (5).

tion of  $\theta_B$ . As can be seen, the pitch-angle cosine range scanned by LEMS30 is nearly always contained in the pitch-angle cosine range scanned by LEFS60. Only when the magnetic vector is close to alignment with the spin axis direction ( $\theta_B < 30^\circ$  or  $\theta_B > 150^\circ$ ) LEMS30 telescope scans a range in  $\mu$  that is unavailable for LEFS60. In Fig. 2 it can also be seen that the  $\mu$ -co values are always higher for LEFS60 than for LEMS30. As expected, the lowest  $\mu$ -co provided by the two telescopes corresponds to the cases when the IMF vector is aligned with the spacecraft spin-axis. In this case, the  $\mu$ -co is around 40% for LEFS60 and 20% for LEMS30. However, in this case it is not possible to obtain any information of the directional distribution of the particles since all sectors measure in the same  $\mu$  range. For  $\theta_B = 90^\circ$  the LEFS60 telescope scans almost all

possible values of  $\mu$  and  $\mu$ -co  $\simeq 100\%$ ;  $\mu$ -co = 80% for LEMS30.

From this section we conclude that, from the point of view of the coverage in pitch-angle cosine, the LEFS60 telescope is more appropriate for electron data analysis than LEMS30, since it provides more information of the directional distribution of the observed particles. When the IMF vector is close to alignment with the spacecraft spin vector, the LEMS30 is scanning a region of the particle PAD that is unavailable for LEFS60. But in this case, as the coverage of the two telescopes is low, the actual directional information contained in the data is very poor for both telescopes. The combination of cross-calibrated telescopes would improve the pitch-angle analysis performed using only a single telescope.

It is important to point out that the electrons measured by LEMS30 are magnetically deflected electrons while LEFS60 uses an aluminized Parylene foil to prevent low-energy protons from entering the detector (Gold et al., 1998). Thus, electron intensities observed by LEMS30 cannot be contaminated by ions, but ions with energies higher than 350 keV approximately can contaminate the LEFS60 electron channels (Gold et al., 1998). In this sense, the LEMS30 telescope provides key information when studying solar near-relativistic electron events. It is possible to qualitatively compare LEMS30 electron measurements to LEFS60 data to check if the LEFS60 data could be contaminated by ions. Similar trends in the spin-averaged intensity profiles observed by the two telescopes are expected if the LEFS60 profiles are not contaminated by ions; small differences may be caused by the fact that the two telescopes sweep different regions of the pitch-angle distribution.

Finally, note that if the IMF vector remains stable during the evolution of an SEP event, the coverage of the telescope is constant throughout the event. The IMF vector, however, does normally vary with time. Then, the  $\mu$ -co of the telescope varies during the observation of the SEP event.

### 3. Coverage influence

In this section we study how the pitch-angle cosine coverage,  $\mu$ -co, of the telescope can change the spin-averaged intensity profiles observed by a telescope on board a spin-stabilized spacecraft for the case of the LEFS60 telescope. We create synthetic observations by using (i) a Monte Carlo transport model to simulate the propagation of near-relativistic electrons along the IMF (Agueda et al., 2008), and (ii) an angular response model of the telescope sectors to transform modeled PADs into sectorized intensities (see Appendix B in Agueda et al. (2008)).

Our calculations of the particle propagation are based on the focused transport model that includes the effects of adiabatic focusing by a diverging Parker spiral magnetic field, the interplanetary scattering by magnetic fluctuations frozen-in into the solar wind, convection with the scattering fluctuations and adiabatic deceleration resulting from the interplay of scattering and focusing (Kocharov et al., 1998; Ruffolo, 1995).

We assume a stable solar wind speed of 400 km/s and that the electron injection takes place at the distance of two solar radii from the center of the Sun. The energy spectrum at the source is assumed to be  $dN/dE \propto E^{-\gamma}$  in the energy range 45–312 keV, with a spectral index  $\gamma = 3$ . We assume that the injection of electrons takes place during two episodes: a short intense episode lasting  $\sim 4$  min and injecting  $3 \times 10^{33}$  electrons, followed by a weaker injection component starting 72 s later and injecting  $3 \times 10^{31}$  electrons. These particles are assumed to be injected into a flux tube that has a cross-section of 1 sr at the source surface. Fig. 3 illustrates the assumed injection profile.

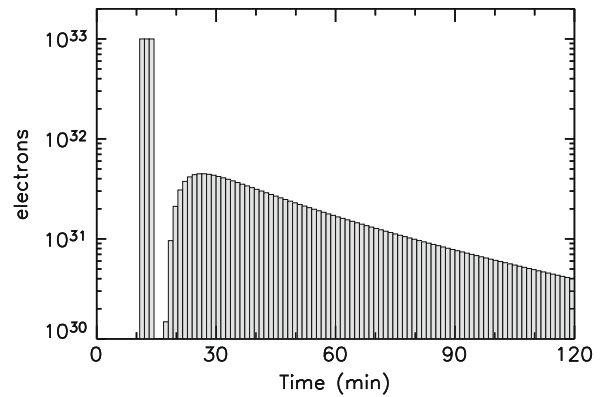


Fig. 3. Two component solar injection profile.

Regarding the transport conditions in the interplanetary medium, we assume isotropic pitch-angle scattering and a constant radial mean free path (see Agueda et al., 2008, for details). We choose two different values of the radial mean free path:  $\lambda_r = 0.9$  AU and  $\lambda_r = 0.1$  AU. This allows us to study both a nearly scatter-free event and an event observed during strong scattering conditions. Note that the transport model provides us with the differential intensities observed at 1 AU and the complete PADs as a function of time.

We assume that these two particle events are observed by a telescope with the characteristics of LEFS60 in a single energy range 175–312 keV (which corresponds to the highest energy channel of EPAM/LEFS60). We use the angular response of the sectors to transform the modeled pitch-angle distributions into sectorized intensities (see Appendix B in Agueda et al. (2008)).

As commented in the previous section, the IMF vector orientation with respect to the spacecraft spin-axis determines the range in pitch-angle cosine seen by the telescope. We assume a stable IMF vector at 1 AU that does not vary with time and select nine configurations that assure five different values of the  $\mu$ -co of the LEFS60 telescope: (1) 40%, (2) 55%, (3) 70%, (4) 85% and (5) 100%. Fig. 2 shows these magnetic field configurations. Each configuration is labeled with a number from 1 to 5; the higher the number the higher the  $\mu$ -co. We assume a positive polarity of the IMF for  $\theta_B \geq 90^\circ$  and a negative polarity for  $\theta_B < 90^\circ$ . Therefore, configurations with  $180^\circ - \theta_B$  are equivalent to configurations with  $\theta_B$ .

Fig. 4 displays the spin-averaged time-intensity profiles that would be observed by LEFS60 for these five IMF configurations. The black profile shows the spin-averaged intensity profile when  $\mu$ -co  $\simeq 100\%$  and the telescope is sampling the whole  $\mu$  range approximately. Note that only in this case, spin-averaged intensities correspond to omnidirectional intensities. We observe that spin-averaged intensities show higher peak intensities and shorter times to maximum than omnidirectional intensities. When  $\lambda_r = 0.9$  AU, the intensity profiles peak in a time interval of  $\sim 1$  min while when  $\lambda_r = 0.1$  AU, the intensity profiles peak in a time interval of  $\sim 5$  min. The relative differences

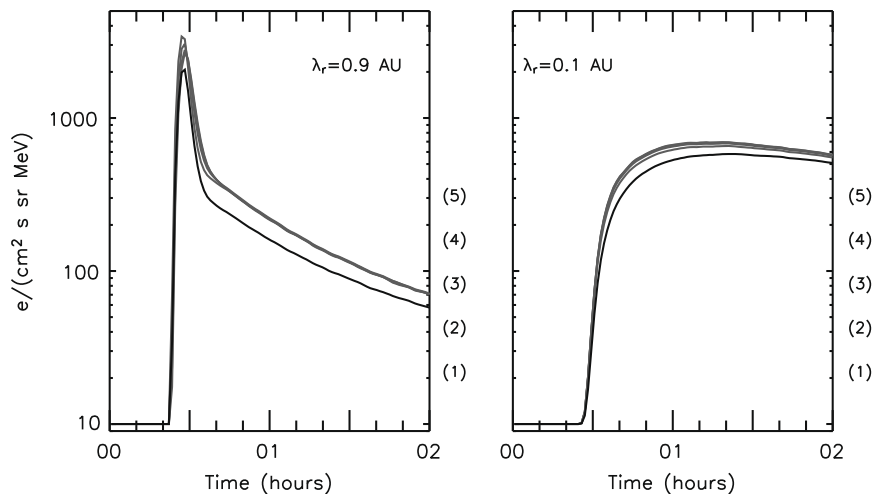


Fig. 4. Spin-averaged intensities observed by the LEFS60 telescope for different magnetic field configurations (see Fig. 2) assuming two different interplanetary transport conditions:  $\lambda_r = 0.9$  AU (left) and  $\lambda_r = 0.1$  AU (right).

between the omni-directional peak intensity and the spin-averaged peak intensities are up to 65% for  $\lambda_r = 0.9$  AU, and 20% for  $\lambda_r = 0.1$  AU.

Thus, an SEP event can display a variety of representations when being observed by a given telescope. These observations can represent an incomplete picture of the actual SEP event since the telescope is not always able to scan complete PADs. Hence, when trying to infer from in situ observations the characteristics of both SEP injection function close to the Sun and the propagation conditions along the IMF, it is important to determine the actual information contained in the data. In the next section, we estimate the  $\mu$ -co required to allow a derivation of the scenario of particle injection and transport from the fit of in situ sectorized electron data.

#### 4. Results

Agueda et al. (2008) presented a new technique for deconvolving in situ particle sectorized intensities allowing us to determine the underlying particle injection profile near the Sun and the transport conditions of SEPs along the IMF. This technique calculates the best-fit injection function by solving a least squares problem between the observed and the modeled sectorized intensities subject to the constrain that the injection function has to be non-negative (see Agueda et al., 2008, for details). The best-fit transport parameters are determined by minimizing the goodness-of-fit estimator  $\zeta = \sum_i (\log O_i - \log M_i)^2$ , where  $O_i$  and  $M_i$  are the observational and modeled sectorized intensities, respectively. The algorithm has been applied to the study of near-relativistic electron events observed by ACE (Agueda et al., 2008).

We now use the same technique to deconvolve synthetic sectorized intensity profiles to study the influence of the  $\mu$ -co of the telescope on the determination of the source function and the transport conditions. We focus on the two interplanetary transport scenarios defined by: (A)  $\lambda_r = 0.9$  AU and (B)  $\lambda_r = 0.1$  AU. Then, by assuming different magnetic

field configurations, we can study how the pitch-angle cosine coverage influences the results of the deconvolution. For this purpose we select the five magnetic field configuration discussed in Section 3, which produce different observational sectorized intensity profiles (see the corresponding spin-averaged intensities in Fig. 4).

We use the interplanetary particle transport model to simulate the propagation of near-relativistic electrons along the IMF for 15 different values of the radial mean free path logarithmically spaced between 0.05 and 1.5 AU. For each value of  $\lambda_r$ , we deconvolve the synthetic observational intensities and obtain the best-fit injection function. Fig. 5 shows the values of the  $\zeta$ -estimator obtained for each  $\lambda_r$ . Row (A) shows the results when the actual radial mean free path is  $\lambda_r = 0.9$  AU and row (B) is for  $\lambda_r = 0.1$  AU. Each column corresponds to a different  $\mu$ -co value of the telescope.

As can be seen, the higher the  $\mu$ -co of the telescope the more symmetric the function  $\zeta(\lambda_r)$  around the best fit value of  $\lambda_r$  and the deeper the minimum. As the radial mean free path becomes smaller than the actual value of  $\lambda_r$ ,  $\lambda_r^a$ , it becomes difficult to reproduce the rising phase of the event. The injection is assumed to start after  $t = 0$ , thus when  $\lambda_r \ll \lambda_r^a$ , particles arrive to the spacecraft too late to reproduce the observed onset. On the other hand, if  $\lambda_r > \lambda_r^a$  the lower the  $\mu$ -co, the flatter the  $\zeta(\lambda_r)$ . For example, when  $\mu$ -co = 40%,  $\zeta(\lambda_r)$  becomes flat (i.e. the estimator takes similar values for a given range of  $\lambda_r$ ). Then, the optimal solution becomes degenerated and there is more than one scenario that reasonably fits the observational data. In this case, the measurements do not allow us to determine univocally  $\lambda_r^a$  and the actual particle injection function close to the Sun. Note that when  $\mu$ -co = 40% all sectors scan nearly the same range of  $\mu$  values. For  $\mu$ -co = 55%,  $\zeta$  also takes similar values in a range of  $\lambda_r$ , which would make difficult to discern the value of  $\lambda_r^a$ .

We have checked that the results of the deconvolution are very similar if, instead of assuming a stable IMF vector,

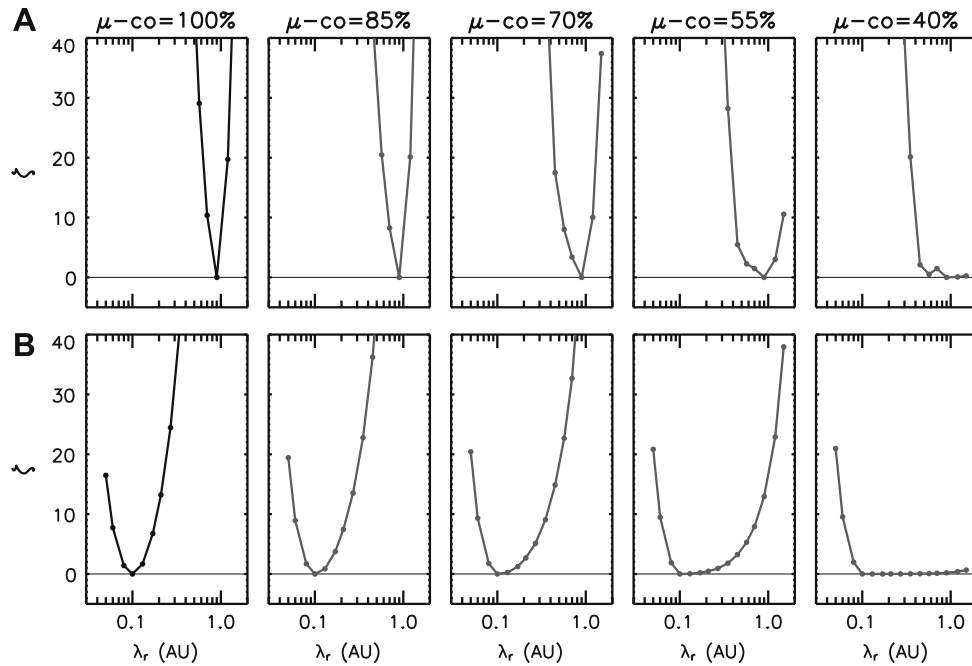


Fig. 5. Goodness of fit estimator obtained for different  $\mu$ -co of the LEFS60 telescope and for different interplanetary transport conditions; (A)  $\lambda_r = 0.9$  AU and (B)  $\lambda_r = 0.1$  AU. The horizontal line marks  $\zeta = 0$ .

variations in the IMF direction are taken into account (Agueda, 2008). Therefore in order to clearly discern the actual value of  $\lambda_r$  and the underlying injection function from LEFS60 sectorized measurements the SEP event must be observed with  $\mu$ -co  $\geq 70\%$ .

## 5. Conclusions

We have quantified the coverage in pitch-angle cosine of two electron telescopes, i.e. LEFS60 and LEMS30, on board the *ACE* spacecraft. We have found that the LEFS60 telescope is more appropriate for electron data analysis than LEMS30, since it provides more information of the directional distribution of the observed particle population.

We have made evident the relevant role that the pitch-angle cosine coverage has when studying SEP events. By studying synthetic electron events, we showed that the spin-averaged time-intensity profiles can display a variety of representations depending on the region of the PAD that the telescope scans for a given IMF configuration. We have set constraints on the conditions under which it is possible to deconvolve the effects of interplanetary particle transport and solar injection on observational intensities. The main conclusion is that in order to discern both the actual interplanetary propagation conditions and the injection profile close to the Sun from LEFS60 measurements the SEP event has to be observed with  $\mu$ -co  $\geq 70\%$ . If  $\mu$ -co is smaller, multiple scenarios can explain the data.

The algorithm and tools developed for the analysis of LEFS60 data can be easily modified and applied to study sectorized time-intensity profiles measured by other tele-

scopes on board spacecraft with similar features and performance (e.g., *Wind*). They could also be adapted to the study of particle measurements made by cross-calibrated telescopes on board three-axis stabilized spacecraft, like *STEREO*. In this case, directional information is provided by several detectors that provide different fields of view.

## Acknowledgments

NA and RV are grateful for the financial support of the Academy of Finland (Projects 110021 and 121650). NA and BS acknowledge financial support from the Ministerio de Ciencia y Tecnología (Spain), under the Projects AYA2004-03022 and AYA2007-60724. DL acknowledges the support from the NSF under the research Grant ATM-0648181 and NASA under HGI Grant NNX09AG30G. Computational support has been provided by the Centre de Supercomputació de Catalunya (CESCA) and the Finnish IT center for science (CSC). NA acknowledges the ESA Education Office for sponsoring her participation in the 37th COSPAR Scientific Assembly.

## References

- Agueda, N. Near-relativistic electron events. Monte Carlo simulations of solar injection and interplanetary transport. Ph.D. Thesis, University of Barcelona, ISBN B.42798-2008/978-84-691-5566-0 (<http://www.tesisenxarxa.net/TDX-0701108-121519/>), 2008.
- Agueda, N., Vainio, R., Lario, D., Sanahuja, B. Injection and interplanetary transport of near-relativistic electrons: modeling the impulsive event on 2000 May 1. *Astrophys. J.* 675, 1601–1613, 2008.
- Gold, R.E., Krimigis, S.M., Hawkins III, S.E., et al. Electron, proton, and alpha monitor on the Advanced Composition Explorer spacecraft. *Space Sci. Rev.* 86, 541–562, 1998.

- Kocharov, L., Vainio, R., Kovaltsov, G.A., Torsti, J. Adiabatic deceleration of solar energetic particles as deduced from monte carlo simulations of interplanetary transport. *Sol. Phys.* 182, 195–215, 1998.
- Lin, R.P., Anderson, K.A., Ashford, S., et al. A three-dimensional plasma and energetic particle investigation for the Wind spacecraft. *Space Sci. Rev.* 71, 125–153, 1995.
- Ng, C.K. Determination of the pitch-angle distribution and transverse anisotropy of interplanetary particles. In: *Proceedings of the 19th ICRC*, vol. 4, La Jolla, pp. 330–333, 1985.
- Ruffolo, D. Effect of adiabatic deceleration on the focused transport of solar cosmic rays. *Astrophys. J.* 442, 861–874, 1995.
- Sanderson, T.R., Reinhard, R., Wenzel, K.P. The propagation of upstream protons between the earth's bow shock and ISEE 3. *J. Geophys. Res.* 86, 4425–4434, 1981.
- Sanderson, T.R., Reinhard, R., van Ness, P., Wenzel, K.P. Observation of three-dimensional anisotropies of 35- to 1000-keV protons associated with interplanetary shocks. *J. Geophys. Res.* 90, 19–27, 1985.